Jpn J Radiol (2014) 32:14–21
DOI 10.1007/s11604-013-0264-y

ORIGINAL ARTICLE

Kurtosis and skewness assessments of solid lung nodule density histograms: differentiating malignant from benign nodules on CT

Ayano Kamiya · Sadayuki Murayama · Hisashi Kamiya · Tsuneo Yamashiro · Yasuji Oshiro · Nobuyuki Tanaka

Received: 5 August 2013 / Accepted: 23 October 2013 / Published online: 19 November 2013

Abstract
Purpose The purpose of our study was to assess pulmonary nodule characteristics using density histogram kurtosis and skewness and to distinguish malignant from benign nodules.
Materials and methods Ninety-three lung nodules on CT were analyzed, including 72 malignant and 21 benign nodules. They were completely solid or solid with limited ground-glass opacity. Based on their CT characteristics, nodules were categorized into type A, homogeneous nodules with uniform internal structures and clear margins, and type B, inhomogeneous nodules with heterogeneous structures or uneven margins. Kurtosis and skewness were calculated from density histograms to compare type A and B nodules and malignant and benign nodules. Receiver-operating characteristic (ROC) curves were generated to assess kurtosis and skewness for discriminating between different nodule types.
Results Type A nodules ($n = 35$) had greater kurtosis and reduced skewness ($p < 0.001$) compared to type B nodules ($n = 58$). Malignant tumor kurtosis was greater than that of benign nodules (type A, $p < 0.05$; type B, $p = 0.001$). Type B malignant tumors had reduced skewness compared to benign nodules ($p < 0.05$). ROC curves provided relatively high values for the area under the curve (0.71–0.83).
Conclusion Kurtosis and skewness assessments of density histograms may be useful for differentiating malignant from benign nodules.

Keywords Computed tomography · Lung nodule · Density histogram · Kurtosis · Skewness

A. Kamiya · S. Murayama · H. Kamiya · T. Yamashiro (✉)
Department of Radiology, Graduate School of Medical Science, University of the Ryukyus, 207 Uehara, Nishihara, Okinawa 903-0215, Japan
e-mail: clatsune@yahoo.co.jp

A. Kamiya
e-mail: ayano1242004@yahoo.co.jp

S. Murayama
e-mail: sadayuki@med.u-ryukyu.ac.jp

H. Kamiya
e-mail: e954123@mail.goo.ne.jp

Y. Oshiro
Department of Radiology, Okinawa National Hospital, National Hospital Organization, 3-20-14 Ganeko, Ginowan, Okinawa 901-2214, Japan
e-mail: oshiro4211@yahoo.co.jp

N. Tanaka
Department of Radiology, Yamaguchi University Graduate School of Medicine, 1-1-1 Minamikogushi, Ube, Yamaguchi 755-8505, Japan
e-mail: nbtanaka@yamaguchi-u.ac.jp

Introduction

Lung cancer is the major cause of cancer-related deaths worldwide with a 5-year survival rate of only 16 % [1]. Diagnosis of lung cancer at an early stage might reduce lung cancer mortality. Recently, the National Lung Screening Trial (NLST) showed that lung cancer death rates could be reduced by 20 % when a high-risk group was screened with low-dose computed tomography (CT) scanning compared to chest radiography [2].

Shortly after the introduction of multidetector-row CT scanners and lung cancer CT screening, there was a dramatic increase in the number of small lung nodules that were detected incidentally. However, most of these nodules

are benign [3–5], which poses a challenge for radiologists to accurately identify the few malignant tumors among the numerous benign nodules [6]. Many of these benign lesions are small solid nodules with difficult histological confirmation, and are usually followed-up to watch for changes in size and shape. High-resolution CT has enabled these nodules to be investigated in greater detail, and analyses of their features, such as contour shape, margins, and internal characteristics, have aided in developing criteria to distinguish malignant from benign nodules [7–9].

Recently, some research groups developed methods to quantify nodule texture on high-resolution CT [10–12]. Kido et al. [10] analyzed the characteristics of lung nodule interfaces using fractal analysis. Nomori et al. and Ikeda et al. reported that a CT histogram was useful for differentiating pathology in nodules with ground-glass opacity (GGO) [11, 12]. Further, Mori et al. [13] demonstrated the advantage of an automated scoring system for contrast enhancement in differentiating malignant and benign lung nodules using dynamic CT. Thin-section CT processing with advanced software has even provided for volume histograms that show detailed distributions of CT values for lung nodules.

Kurtosis and skewness are representative, basic indices that can be obtained from density histograms. They represent the distortion or disparity deviation of a histogram when compared with a normal distribution. Several studies have used these indices to evaluate various lung diseases, as these parameters can be measured easily using open-source or commercial software [14, 15]. However, to the best of our knowledge, there is no published information on kurtosis and skewness measures for CT-based density histograms of lung nodules. Previous studies that discussed density histograms of lung nodules evaluated mean/peak CT values and percentile values of the histograms only [11, 12]. Thus, information on kurtosis and skewness measurements of lung nodules remains uncertain, although these indices can be determined on plain chest CT.

Based on previous studies regarding various lung conditions [14, 15], it would be expected that measuring the kurtosis and skewness of density histograms would provide meaningful information on the characteristics of lung nodules, in particular regarding density homogeneity or heterogeneity of the targeted nodules. Therefore, we hypothesized that (1) at least non-uniform and uniform nodules could be discriminated using kurtosis and skewness analysis and (2) these measures could also be extended to differentiating between malignant and benign nodules. Thus, the purpose of this study was to assess lung nodule characteristics using kurtosis and skewness measurements of CT-based density histograms and to examine whether these indices could be used to distinguish malignant from benign nodules.

Materials and methods

This study was approved by the institutional review boards of the three participating institutions. Informed consent was waived as this was a retrospective review of patient records and images.

Subjects

Ninety-three subjects (54 men, 39 women; average age, 67.3 ± 12.1 years; age range 15–86 years) with solid lung nodules (72 malignant and 21 benign nodules) were enrolled from September 2000 to December 2010 in two institutions and from January 2009 to December 2010 in the third. At each institution, consecutive subjects who fulfilled the following criteria were enrolled in this study: (1) plain chest CT (section thickness $\leq$2 mm) was performed for clinical indications; (2) a solid pulmonary nodule (8–20 mm in diameter) without obvious calcification or necrosis was depicted on CT; (3) the final pathological or clinical diagnosis for each nodule characteristic (malignant or benign) was available in the medical record. These subjects were identified by board-certified radiologists at each institution (A.K., Y.O., and N.T. with 7, 19, and 24 years of experience in chest imaging, respectively).

Because this study targeted solid nodules only, nodules displaying $\geq$25 % GGO on the maximum axial section were not included. The nodules were diagnosed as benign if they disappeared, were reduced in size after follow-up, or showed no change after 2 years.

Ultimately, 72 malignant nodules were identified, including adenocarcinoma ($n = 45$), squamous cell carcinoma ($n = 15$), small cell carcinoma ($n = 4$), large cell carcinoma ($n = 1$), and solitary pulmonary metastases ($n = 7$). Twenty-one nodules were eventually diagnosed as benign, including disappearance or reduction in size ($n = 13$), no change after 2 years ($n = 5$), pathologically proven inflammatory nodules ($n = 2$), and one sclerosing hemangioma.

CT scans

CT scanning was performed with multiple scanners at three institutions over the entire 11-year period: 'SOMATOM Plus' and 'SOMATOM Volume Zoom' with 4-row detectors; 'SOMATOM Definition' and 'SOMATOM Sensation' with 64-row detectors (Siemens Healthcare, Erlangen, Germany); 'Lightspeed QX/I' with 4-row detectors; 'Lightspeed VCT' with 64-row detectors (GE Medical Systems, Milwaukee, WI, USA); 'Aquilion 4' with 4-row detectors; 'Aquilion 64' with 64-detectors; 'Aquilion ONE' with 320-row detectors (Toshiba Medical Systems,

Table 1 CT scanners and settings

Scanner (detector row)	Manufacturer	Patient number	Voltage (kVp)	Tube current (mA)	Rotation time (sec)	Kernel	Section thickness (mm)
SOMATOM plus (4)	Siemens	13	120	200	0.75	AB50	2
SOMATOM volume zoom (4)	Siemens	16	140	320	0.75	B70s	2
SOMATOM Definition (64)	Siemens	14	120	AEC	0.5	B70f	2
SOMATOM sensation (64)	Siemens	19	120	AEC	0.5	B70f	2
Lightspeed QX/I (4)	GE	6	120 or 140	250–280	0.8	Lung	1.25
Lightspeed VCT (64)	GE	4	120	AEC	0.4	Chest or bone plus	1.25
Aquilion 4 (4)	Toshiba	16	120	300	0.5	FC50	2
Aquilion 64 (64)	Toshiba	4	120	AEC	0.5	FC86	1 or 2
Aquilion ONE (320)	Toshiba	1	120	AEC	0.5	FC51	1

AEC automatic exposure control

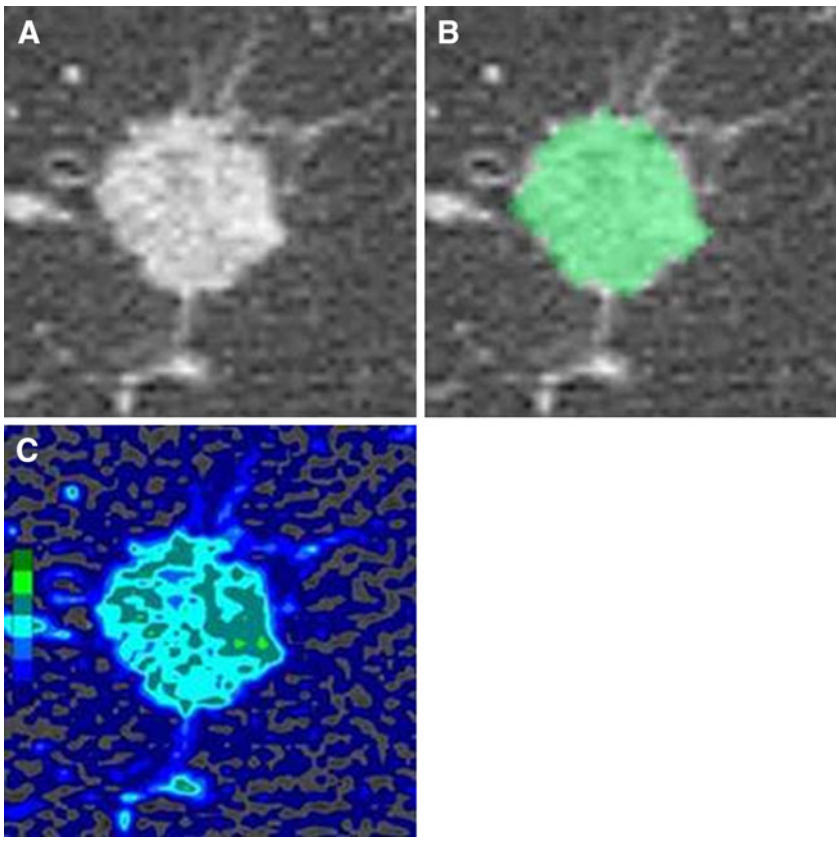

Fig. 1 Nodule contouring process. **a** An adenocarcinoma with a heterogeneous internal structure and an irregular margin (type B). **b** The margin of the nodule is traced manually, and the nodule is segmented. **c** A *color* mapping image shows various *colors* in the segmented nodule, which represent the heterogeneous CT density of the nodule

Otawara, Tochigi, Japan). Detailed information on the scanning and reconstruction settings is shown in Table 1. In brief, these parameters were: tube voltage of 120 or 140 kVp; tube current of 200–320 mA or automatic exposure control (range 100–550 mA); rotation time of 0.4–0.8 s; 512 × 512 matrix size; a slice thickness of ≤2 mm. No patient had received intravenous contrast medium. Images were reconstructed with an edge-enhancing kernel, such as the 'lung' kernel for GE scanners and the 'FC 86' kernel for Toshiba scanners.

Image analysis

All CT image sets were transferred to a commercial workstation (Vincent version 2.4, Fujifilm Medical, Tokyo, Japan) for histogram analysis. CT images were displayed with a window level of −500 Hounsfield units (HU) and a window width of 1,500 HU. Software integrated in the workstation was used by one radiologist (A.K.) to contour each targeted nodule on all axial CT images that included the nodule. Another radiologist (H.K.) with 11 years of

experience verified the contour accuracy. After outlining the nodule on all images, the workstation created a density histogram of the entire nodule using a volumetric (three-dimensional) approach. Two-dimensional color mapping, which reflected CT values, was automatically delineated to visualize the density (Fig. 1).

Nodules were classified into two types based on their internal and marginal properties. Type A was homogeneous solid nodules with uniform internal structures and clear margins (Fig. 2). Type B was inhomogeneous solid nodules with heterogeneous internal structures or uneven margins (Fig. 3). Two radiologists (A.K. and H.K.) independently determined the types based on the traced margins and the nodules' color mappings, without information on kurtosis and skewness values. When their results did not agree, a consensus was reached.

For quantitative evaluations, kurtosis and skewness were automatically determined from the volumetric density histogram by the workstation. Briefly, kurtosis describes how sharply peaked a histogram is; a normal distribution has a kurtosis of zero, whereas a histogram that is more peaked than a normal distribution has a positive kurtosis value. Skewness describes the degree of asymmetry of a histogram; a completely symmetrical distribution has a skewness value of zero, whereas a histogram with a long tail to the right has a positive skewness value [14, 15].

Intraobserver error of the qualitative CT measures was tested by having one observer (A.K.) trace the nodule margin and measure kurtosis and skewness twice for 35 nodules, which were randomly selected from a total of 93 nodules. The second measurement was performed 6 months after the first session. To evaluate interobserver error, two observers (A.K. and H.K.) independently contoured the 35 nodules and measured these values.

Statistical analysis

Statistical analysis was performed using JMP 8.0 software (SAS Institute, Cary, NC, USA). Cohen's kappa coefficient (κ-value) was determined to assess the interobserver agreement for nodule characteristics (type A or B) [16]. Interobserver agreement was considered as slight ($\kappa < 0.21$), fair ($\kappa = 0.21$–0.40), moderate ($\kappa = 0.41$–0.60), substantial ($\kappa = 0.61$–0.80), and almost perfect ($\kappa = 0.81$–1.00). Analysis of intra- and interobserver reproducibility for the quantitative analyses was conducted using Bland-Altman analysis.

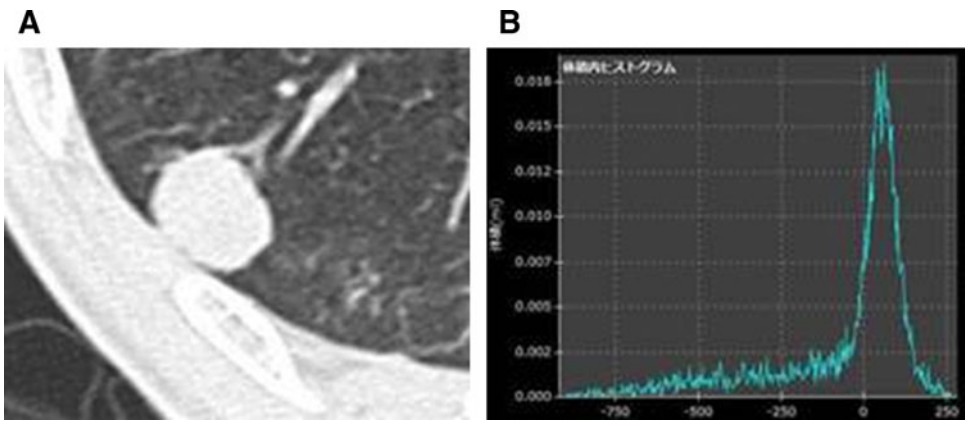

Fig. 2 Analysis of a small cell carcinoma in a 59-year-old man. **a** This nodule is homogeneous with a clear boundary and classified as type A. **b** The histogram for this nodule has a very steep peak

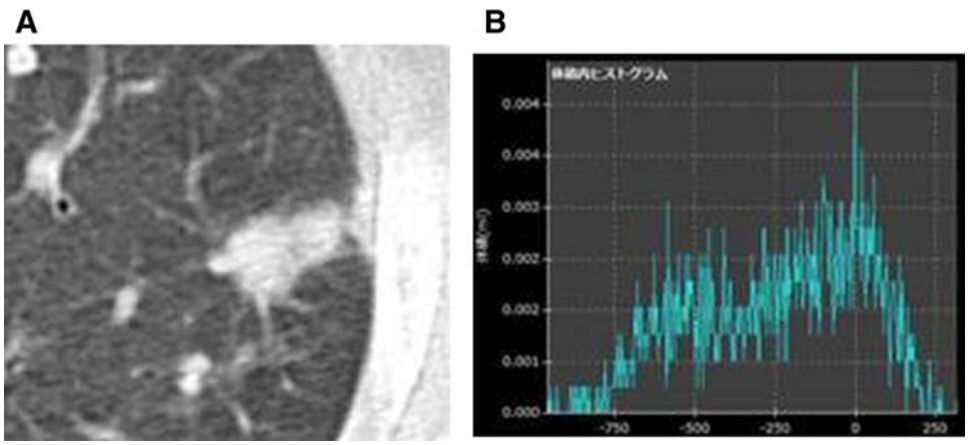

Fig. 3 A clinically diagnosed benign nodule in a 72-year-old woman. **a** This nodule is heterogeneous with an indeterminate boundary and classified as type B. **b** Histogram analysis shows a flattened peak and a long left tail

Comparisons of nodule size and histogram measurements between type A and B nodules and between malignant and benign nodules were made by Mann-Whitney U tests. Receiver-operating characteristic curve (ROC) analysis was used to determine how well kurtosis and skewness could discriminate nodules. We calculated the ROC area under the curve (AUC) and determined sensitivity and specificity based on cutoff values obtained from ROC analysis. Also, the accuracy, positive predictive value (PPV), and negative predictive value (NPV) were obtained from the ROC analysis. *P* values of <0.05 were considered significant.

Results

Nodule classification

The interobserver agreement for classifying nodule types was excellent ($\kappa = 0.84$). Of 93 nodules evaluated, 35 were classified as type A, including 24 malignant nodules (9 adenocarcinoma, 6 squamous cell carcinoma, 4 small cell carcinoma, 1 large cell carcinoma, and 4 solitary pulmonary metastases) and 11 benign nodules (9 clinically diagnosed, 1 sclerosing hemangioma, and 1 pathologically proven inflammatory nodule). Based on histogram analysis, these nodules displayed characteristic sharp peaks (Fig. 2). Type B nodules ($n = 58$) included 48 malignant nodules (36 adenocarcinomas, 9 squamous cell carcinoma, 3 solitary pulmonary metastases) and 10 benign nodules (9 clinically diagnosed and one pathologically proven inflammatory nodule). Their histograms showed multiple peaks or a single flat peak (Fig. 3). No significant differences in nodule size were found between type A and B nodules (type A, 13.7 ± 2.6 mm; type B, 14.0 ± 3.3 mm) or between malignant and benign nodules (malignant, 13.2 ± 3.3 mm; benign, 14.1 ± 3.0 mm).

Histogram analysis

Table 2 shows the quantitative results of the nodule histogram analyses. Type A nodules had significantly greater kurtosis ($p < 0.001$) and reduced skewness ($p < 0.001$) compared to type B nodules. When combining type A and B nodules, kurtosis and skewness did not significantly differ between malignant and benign nodules. However, for each type, the kurtosis of malignant nodules was significantly greater than that of benign nodules (type A, $p < 0.05$; type B, $p = 0.001$). The skewness of malignant type B nodules was also significantly reduced compared to benign nodules ($p < 0.05$).

Kurtosis had a good capability to differentiate nodules, with an AUC of 0.71 for type A and 0.83 for type B (Figs. 4, 5). Using a kurtosis threshold of 1.57 for type A, the sensitivity and specificity were 83.3 and 63.6 %, respectively. The accuracy, PPV, and NPV were 77.1, 83.3, and 50.0 %, respectively. A kurtosis threshold of −0.38 for

Table 2 Quantitative histogram analysis

Nodule characteristics	Kurtosis		Skewness	
	Mean ± SD	*P* value	Mean ± SD	*P* value
All nodules ($n = 93$)	0.95 ± 1.78	–	−1.04 ± 0.60	–
Type A ($n = 35$)	2.29 ± 1.72	<0.001	−1.49 ± 0.40	<0.001
Type B ($n = 58$)	0.13 ± 1.25		−0.78 ± 0.55	
All nodules		NS (0.18)		NS (0.06)
Malignant ($n = 72$)	0.42 ± 1.75		−1.09 ± 0.61	
Benign ($n = 21$)	1.10 ± 1.77		−0.89 ± 0.58	
Type A		<0.05		NS (0.09)
Malignant ($n = 24$)	2.65 ± 1.59		−1.55 ± 0.41	
Benign ($n = 11$)	1.51 ± 1.80		−1.34 ± 0.35	
Type B		0.001		<0.05
Malignant ($n = 48$)	0.33 ± 1.29		−0.85 ± 0.55	
Benign ($n = 10$)	−0.77 ± 0.44		−0.48 ± 0.34	

SD standard deviation, *NS* not significant

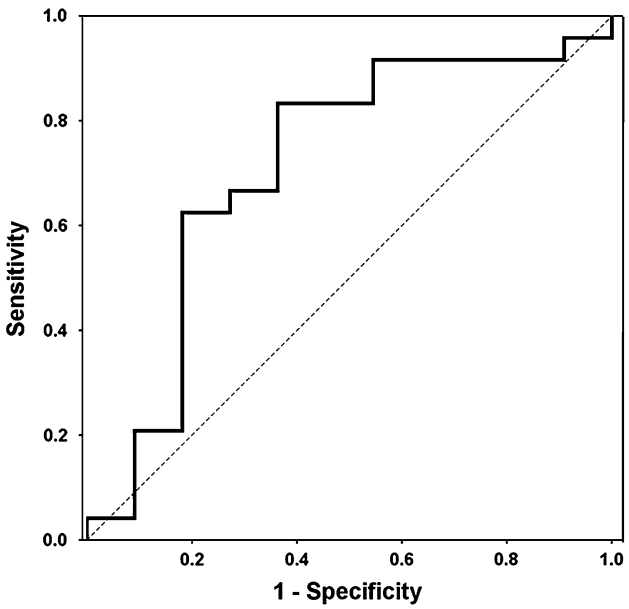

Fig. 4 ROC curve for kurtosis in type A for differentiating malignant from benign nodules. Kurtosis demonstrated good performance for differentiating malignant from benign nodules with an AUC of 0.71

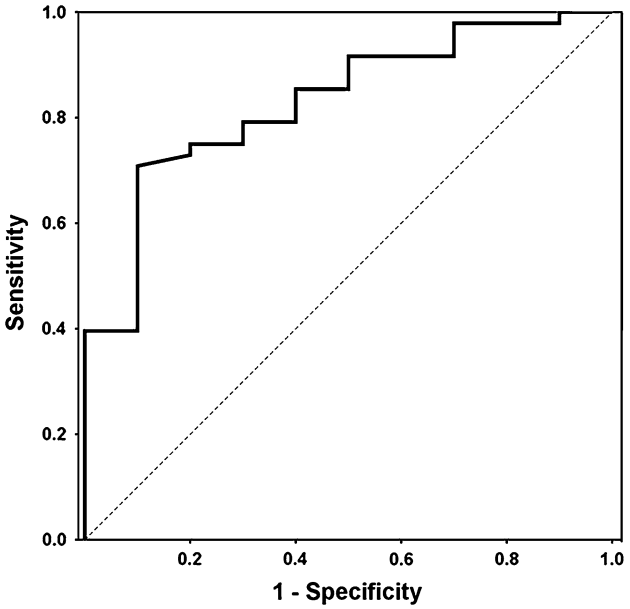

Fig. 5 ROC curve for kurtosis in type B for differentiating malignant from benign nodules. Kurtosis demonstrated good performance for differentiating malignant from benign nodules with an AUC of 0.83

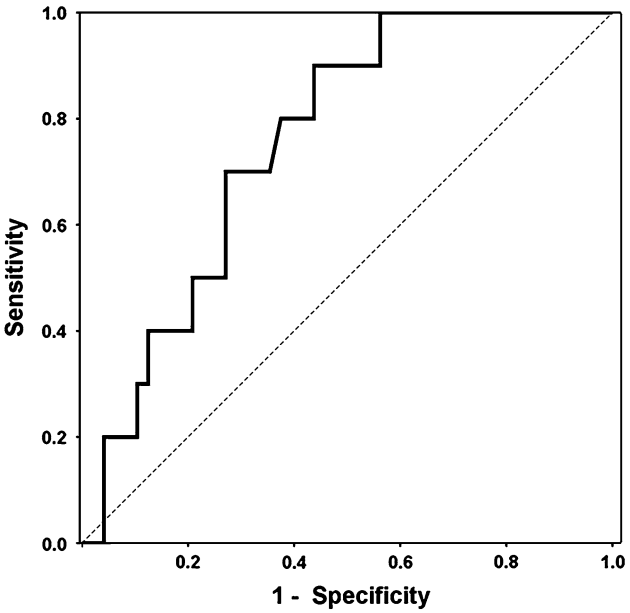

Fig. 6 ROC curve for skewness in type B for differentiating malignant from benign nodules. Skewness demonstrated good performance for differentiating malignant from benign nodules with an AUC of 0.76

type B provided a sensitivity and specificity of 70.8 and 90 %, respectively. The accuracy, PPV, and NPV were 74.1, 97.1, and 93.3 %, respectively. Skewness had a good capability for nodule differentiation with an AUC of 0.76 for type B (Fig. 6). A skewness threshold of −0.77 for type B provided a sensitivity of 56.3 %, specificity of 90 %, accuracy of 62.1 %, PPV of 96.4 %, and NPV of 95.5 %.

Table 3 Intra- and interobserver reproducibility of kurtosis and skewness measurements

	Mean difference ± SD	Limit of agreement
Intraobserver error		
Kurtosis	0.00 ± 0.22	−0.44 to 0.45
Skewness	0.00 ± 0.04	−0.09 to 0.08
Interobserver error		
Kurtosis	0.17 ± 0.57	−0.97 to 1.31
Skewness	−0.06 ± 0.11	−0.29 to 0.16

SD standard deviation

The intra- and interobserver variability for kurtosis and skewness measurements are shown in Table 3. The mean difference did not appreciably deviate from zero, and the limits of agreement were small.

Discussion

Chest CT histogram analysis has been used to evaluate the properties of several pulmonary diseases, including interstitial lung disease, pulmonary embolisms, and pulmonary nodules [11, 12, 14, 15, 17–20]. With regard to CT values of lung nodules, some studies used histograms to detect an average CT level or a peak CT level for differentiating several types of neoplastic lesions, such as bronchioloalveolar carcinoma (adenocarcinoma in situ), atypical adenomatous hyperplasia, and adenocarcinoma [11, 12, 21]. However, no previous report used kurtosis or skewness measures for evaluating lung nodules, although these indices are easily determined from density histograms. We characterized pulmonary nodules based on their kurtosis and skewness observed on density histograms and found that this method could effectively evaluate nodule characteristics, including predicting malignant or benign nodules. Based on our findings, when solid pulmonary nodules are detected on chest CT, histogram analysis is recommended to obtain latent information on internal density homogeneity, which may be useful for differentiating malignant from benign nodules.

Type A nodules are thought to include malignant nodules that exhibit bulging growth patterns and benign tumors with clear boundaries or capsules, such as hamartoma, inflammatory nodules (partial atelectasis and granuloma), and intrapulmonary lymph nodes. Actual type A malignant nodules include various types of lung cancer, such as adenocarcinomas, squamous cell carcinoma, small cell carcinoma, large cell carcinoma, and solitary pulmonary metastases. Fifteen malignant tumors other than adenocarcinomas showed a typical expanding growth pattern on CT scans [22]. Although a detailed pathological assessment was not performed in this study, adenocarcinomas of this

type would be pathologically classified as papillary or poorly differentiated, which usually show expanding (bulging) growth [4, 22]. Also, 11 benign nodules of type A included 5 nodules without changes in size for 2 years, which may have been granulomas or intrapulmonary lymph nodes rather than temporary pulmonary inflammation.

By comparison, type B nodules are thought to include malignant tumors with invasive growth patterns (or adenocarcinomas showing lepidic growth) and benign inflammatory nodules without clear boundaries [4, 22, 23]. Actual malignant type B nodules included 75 % (36 of 48) adenocarcinomas, which were thought to be mostly classified as a lepidic growth type. Nine of ten benign nodules of type B had disappeared or were reduced in size on follow-up CT scans, suggesting that they were temporary inflammatory lesions and that their actual internal structures were less solid than type A benign nodules.

In the histogram analysis for each group, a significant difference was found in the kurtosis values between benign and malignant nodules of type A. Similar significant differences in kurtosis and skewness were found for type B nodules. Greater kurtosis (type A and B) or reduced skewness (type B) was found for malignant nodules, and the ROC analyses using these indices were satisfactory. Although it is very difficult to speculate on the exact reasons for the greater kurtosis and reduced skewness for malignant nodules, the following explanation is plausible. In type A malignant nodules, the internal cells and interstitium are considered to be uniformly arranged in the nodule tissue, which would result in mostly similar CT values and a single, steep peak in the density histogram. Conversely, reduced kurtosis for type A benign nodules indicates that their internal structure is more heterogeneous than malignant nodules, although they appear to be uniform solid nodules on CT images. These differences in internal density homogeneity would be reflected by the differences in kurtosis measurements between malignant and benign nodules of type A, which would not be detected by conventional visual assessments. For type B nodules, most malignant nodules (75 %) were adenocarcinoma. The central region of an adenocarcinoma with lepidic growth is considered to be comparatively uniform, and the surrounding part shows a gradual increase in CT values on a density histogram. In this situation, a density histogram for an adenocarcinoma typically shows a clear, single peak with wider slopes. Conversely, the internal structures of inflammatory nodules of type B are more heterogeneous than malignant nodules, which would result in multiple density peaks or no definite peak in a histogram, and further reduce the kurtosis and increase skewness relative to malignant nodules. However, it remains unknown whether these characteristics of lung nodules were truly correct for the nodules targeted in this study, as we did not perform a histopathological analysis. Therefore, these explanations should be considered as speculative.

This study had several limitations. A major limitation was that our cases were retrospectively selected from three institutions over 11 years and using various CT scanners, which created differences in the scanning and reconstruction methods. Although slice thickness, tube voltage, and tube current were controlled, differences in other parameters may have biased our data to some extent. Further, sharper reconstruction kernels would not have been appropriate for quantitative density analyses. Second, there were fewer benign nodules than malignant nodules. We limited the size of nodules to over 8 mm in maximum diameter, which are recommended for frequent follow-up CT by the Fleischner Society [24]. Smaller benign nodules between 5 mm and 8 mm may also have been appropriate for our analysis. However, in a report on the variability of CT lung nodule volumetry to determine the minimum change needed to detect the growth of solid lung nodules, variability was significantly less for nodules of greater than 8 mm in diameter [25]. Therefore, our study on volume data was limited to those nodules over 8 mm in diameter. Third, nodular margins were traced by a single operator and verified by another observer. When a portion with a very low CT value exists in a nodular margin, the accuracy of tracing may be inaccurate. Fourth, our aim was not to investigate the effects of kurtosis-skewness measurements for daily clinical management of lung nodules. Thus, we did not assess whether or not these histogram measurements would actually aid radiologists in distinguishing malignant and benign nodules when these quantitative measurements are added to conventional subjective assessments. This should be investigated in future studies.

In conclusion, kurtosis and skewness values determined from density histogram analysis of chest CT images have the potential to differentiate between malignant and benign lung nodules, which may be a new quantitative diagnostic approach for solid lung nodules.

Conflict of interest There is no conflict of interest regarding the manuscript.

References

1. Siegel R, Ward E, Brawley O, Jemal A. Cancer statistics, 2011: the impact of eliminating socioeconomic and racial disparities on premature cancer deaths. CA Cancer J Clin. 2011;61:212–36.
2. National Lung Screening Trial Research Team, Aberle, Adams AM, Berg CD, Black WC, Clapp JD, et al. Reduced lung-cancer mortality with low-dose computed tomographic screening. N Engl J Med. 2011;365:395–409.
3. Henschke CI, Yankelevitz DF, Mirtcheva R, McGuinness G, McCauley D, Miettinen OS, et al. CT screening for lung cancer:

frequency and significance of part-solid and nonsolid nodules. AJR Am J Roentgenol. 2002;178:1053–7.
4. Yang ZG, Sone S, Takashima S, Li F, Honda T, Maruyama Y, et al. High-resolution CT analysis of small peripheral lung adenocarcinomas revealed on screening helical CT. AJR Am J Roentgenol. 2001;176:1399–407.
5. Takashima S, Sone S, Li F, Maruyama Y, Hasegawa M, Matsushita T, et al. Small solitary pulmonary nodules (< or = 1 cm) redetected at population-based CT screening for lung cancer: reliable high-resolution CT features of benign lesions. AJR Am J Roentgenol. 2003;180:955–64.
6. Bach PB. Reduced lung-cancer mortality with CT screening. N Engl J Med. 2011;365:2036.
7. Kuriyama K, Tateishi R, Doi O, Higashiyama M, Kodama K, Inoue E, et al. Prevalence of air bronchograms in small peripheral carcinomas of the lung on thinsection CT. AJR Am J Roentgenol. 1991;156:921–4.
8. Kuriyama K, Seto M, Kasugai T, Higashiyama M, Kido S, Sawai Y, et al. Ground-glass opacity on thin-section CT: value in differentiating subtypes of adenocarcinoma of the lung. AJR Am J Roentgenol. 1999;173:465–9.
9. Takashima S, Maruyama Y, Hasegawa M, Yamanda T, Honda T, Kadoya M, et al. Prognostic significance of high-resolution CT findings in small peripheral adenocarcinoma of the lung: a retrospective study on 64 patients. Lung Cancer. 2002;36:289–95.
10. Kido S, Kuriyama K, Higashiyama M, Kasugai T, Kuroda C. Fractal analysis of small peripheral pulmonary nodules in thinsection CT: evaluation of the lung-nodule interfaces. J Comput Assist Tomogr. 2002;26:573–8.
11. Nomori H, Ohtsuka T, Naruke T, Suemasu K. Differentiating between atypical adenomatous hyperplasia and bronchioloalveolar carcinoma using the computed tomography number histogram. Ann Thorac Surg. 2003;76:867–71.
12. Ikeda K, Awai K, Mori T, Kawanaka K, Yamashita Y, Nomori H. Differential diagnosis of ground-glass opacity nodules: CT number analysis by three-dimensional computerized quantification. Chest. 2007;132:984–90.
13. Mori K, Niki N, Kondo T, Kamiyama Y, Kodama T, Kawada Y, et al. Development of a novel computer-aided diagnosis system for automatic discrimination of malignant from benign solitary pulmonary nodules on thin-section dynamic computed tomography. J Comput Assist Tomogr. 2005;29:215–22.
14. Matsuoka S, Kurihara Y, Yagihashi K, Niimi H, Nakajima Y. Quantification of thin-section CT lung attenuation in acute pulmonary embolism: correlations with arterial blood gas levels and CT angiography. AJR Am J Roentgenol. 2006;186:1272–9.
15. Yamashiro T, Matsuoka S, San Jose Estepar R, Bartholmai BJ, Diaz A, Ross JC, et al. Kurtosis and skewness of density histograms on inspiratory and expiratory CT scans in smokers. COPD. 2011;8:13–20.
16. Sim J, Wright CC. The kappa statistic in reliability studies: use, interpretation, and sample size requirements. Phys Ther. 2005;85:257–68.
17. Sumikawa H, Johkoh T, Yamamoto S, Yanagawa M, Inoue A, Honda O, et al. Computed tomography values calculation and volume histogram analysis for various computed tomographic patterns of diffuse lung diseases. J Comput Assist Tomogr. 2009;33:731–8.
18. Koyama H, Ohno Y, Yamazaki Y, Nogami M, Kusaka A, Murase K, et al. Quantitatively assessed CT imaging measures of pulmonary interstitial pneumonia: effects of reconstruction algorithms on histogram parameters. Eur J Radiol. 2010;74:142–6.
19. Orlandi I, Camiciottoli G, Diciotti S, Bartolucci M, Cavigli E, Nacci F, et al. Thin-section and low-dose volumetric computed tomographic densitometry of the lung in systemic sclerosis. J Comput Assist Tomogr. 2006;30:823–7.
20. Best AC, Lynch AM, Bozic CM, Miller D, Grunwald GK, Lynch DA. Quantitative CT index in idiopathic pulmonary fibrosis: relationship with physiologic impairment. Radiology. 2003;228:407–14.
21. Kawata Y, Niki N, Ohmatsu H, Kusumoto M, Tsuchida T, Eguchi K, et al. Quantitative classification based on CT histogram analysis of non-small cell lung cancer: correlation with histopathological characteristics and recurrence-free survival. Med Phys. 2012;39:988–1000.
22. Hasegawa M, Sone S, Takashima S, Li F, Yang ZG, Maruyama Y, et al. Growth rate of small lung cancers detected on mass CT screening. Br J Radiol. 2000;73:1252–9.
23. Noguchi M, Morikawa A, Kawasaki M, Matsuno Y, Yamada T, Hirohashi S, et al. Small adenocarcinoma of the lung. Histologic characteristics and prognosis. Cancer. 1995;75:2844–52.
24. MacMahon H, Austin JH, Gamsu G, Herold CJ, Jett JR, Naidich DP, et al. Guidelines for management of small pulmonary nodules detected on CT scans: a statement from the Fleischner Society. Radiology. 2005;237:395–400.
25. de Hoop B, Gietema H, van Ginneken B, Zanen P, Groenewegen G, Prokop M. A comparison of six software packages for evaluation of solid lung nodules using semi-automated volumetry: what is the minimum increase in size to detect growth in repeated CT examinations. Eur Radiol. 2009;19:800–8.